UNIVERSITÀ DEGLI STUDI DI PISA

Facolta di Scienze Matematiche Fisiche e Naturali

Corso di Laurea in

FISICA

Researches on non-standard optics for advanced G.W. interferometers.

Tesina del secondo anno di Dottorato ($XVIII^{\circ}$ ciclo)

(Annual status report to the Doctoral School Board)

Juri Agresti

Relatore interno:

Prof. F. Fidecaro

Relatore esterno:

Dr. R. DeSalvo

Anno Accademico 2004-2005

LIGO-T040225-00-R

1 Introduction

The internal thermal noise of the test masses is one of the most important noise source limiting the sensitivity of advanced interferometric gravitational-wave detectors [4] in the frequency range from $\sim$ 40Hz to $\sim$ 200Hz (Cf. Fig. 1): a fluctuational redistribution of thermal energy inside the mirrors produces a fluctuational change of test mass's shape and a change of the position of its reflecting surface, which is undistinguishable from a gravity-wave-induced motion of the test mass's center of mass. This is one of the fundamental limits of gravitational waves detector interferometers.

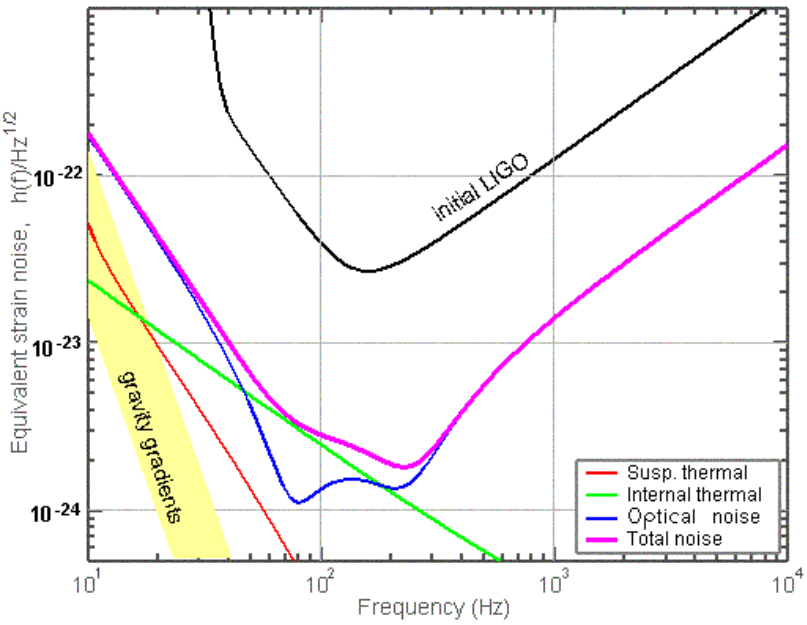

Figure 1: Advanced LIGO design sensitivity (sapphire substrate) and fundamental limitations.

There are various types of internal thermal noise, each one associated with a specific dissipation mechanism. The relative importance of one with respect to the other is determined by the mechanical and thermodynamical properties of the test mass materials.
Homogeneous thermal noise [11] is due to intrinsic losses in the substrate material and is associated with all forms of dissipation that are describable by an imaginary part of the Young's modulus as long as dissipation is uniform inside the substrate of the test masses.
Thermoelastic noise [9] is created by the stochastic flow of heat within each test mass, producing fluctuations of temperature; due to the thermal expansion coefficient, the test-mass material expands in the hot spots and contract in the cold spots, creating fluctuating bumps and valleys on the mirror faces.
It has been recently pointed out that it is critically important how the losses are

distributed inside the test masses. Losses far from the beam spot contribute little to the total thermal noise, whereas losses near the spot, in the dielectric coating for example, contribute more.
Coating thermal noise [12] due to internal losses or to thermoelastic-damping [13] is thought to be the dominant contribution to the thermal noise for mirrors with a SiO_2/Ta_2O_5 coating on a fused silica substrate, whereas the thermoelastic noise of the substrate is the dominant contribution for sapphire mirrors.
The position of the mirror's surface is measured with interferometric techniques. The surface fluctuations produced by thermal noise are averaged by the intensity distribution of the laser beam over the mirror surface. The standard design of interferometers uses light beams with a Gaussian distribution of power, which are eigenfunctions of cavities with spherical mirrors, a well-developed and understood technology. Many authors analyzed the influence of the beam radius r_0 (radius at which the power drops down by a factor $\frac{1}{e}$) on the different types of thermal noise for Gaussian beams. They found the following scaling rules for the noise spectral densities when the mirror is considered as an infinite half-space:

$$\begin{aligned} S_h^{TE-s} &\propto \frac{1}{r_0^3} && \text{Substrate thermoelastic noise} \\ S_h^{TE-c} &\propto \frac{1}{r_0^2} && \text{Coating thermoelastic noise} \\ S_h^{B-s} &\propto \frac{1}{r_0} && \text{Substrate Brownian noise} \\ S_h^{B-c} &\propto \frac{1}{r_0^2} && \text{Coating Brownian noise} \end{aligned}$$

The larger is the beam radius r_0, the better is the averaging of the fluctuations and thus lower will be the noise. However the beam size is constrained by the diffraction losses requirement ($\sim ppm$). It has been argued [1],[2],[3] that a significant reduction in mirror's thermal noise can be achieved by using modified optics that reshape the beam from a conventional Gaussian profile into a Flat-Top ("mesa-beam") profile. A large-radius, flat-topped beam with steep edges (necessary to keep small diffraction losses) will lead to a better sampling of the fluctuating surface and this will result in a lower noise in the determination of the mirror surface position. This in its turn leads to larger sensitivity of the gravitational waves detector.

2 Duality relation between non-spherical cavities

In this section I present a work done in collaboration with Erika D'Ambrosio about a generalization of the duality relation between optical resonators with non spherical mirrors [8], [7]. We demonstrate that there is a one-to-one correspondence between the eigenstates and the eigenvalues of cavities obtained modifying flat mirror cavities by $h(\vec{r})$ and cavities modified from concentric mirrors by $-h(\vec{r})$. This unique mapping

is useful for studying practical issues related to advanced interferometers using non-Gaussian optics, but also in a variety of other applications of Fabry-Perot cavities. Let's focus on the propagator $\mathcal{K}$ from *the surface* of one mirror to the *surface* of the other to find the eigenvalues γ and eigenmodes $v(\vec{r})$ (field distribution over the mirror surface) of a symmetric cavity. The integral equation defining the modes of this system can be derived from Fresnel-Kirchhoff diffraction theory. Our development is based on the general formalism defined in [5] and [6]. We start with

$$\gamma v(\vec{r}) = \int_{Mirror} \mathrm{d}^2\vec{r}\,'\mathcal{K}(\vec{r},\vec{r}\,')v(\vec{r}\,') \tag{1}$$

where the 2-D vectors $\vec{r}$ and $\vec{r}\,'$ are the coordinates of the projections of mirror-surface points on planes orthogonal to the cavity axis at the mirrors positions. The kernel

$$\mathcal{K}(\vec{r},\vec{r}\,') = \frac{ik}{4\pi\rho}(1+\cos\theta)e^{-ik\rho} \qquad\qquad k = \frac{2\pi}{\lambda}$$

depends on the distance ρ between any pair of points on the two surfaces (see fig. 8). Such distance depends on both the surface profiles, which are assumed to be the same throughout our analysis

$$\rho = \sqrt{\delta^2 + |\vec{r}-\vec{r}\,'|^2} \qquad \delta = L - h(\vec{r}) - h(\vec{r}\,') \tag{2}$$

where the reference surface from which the mirror height $h(\vec{r})$is measured, is flat and orthogonal to the optical axis of the cavity, and the origin passes through the centers of the mirrors.

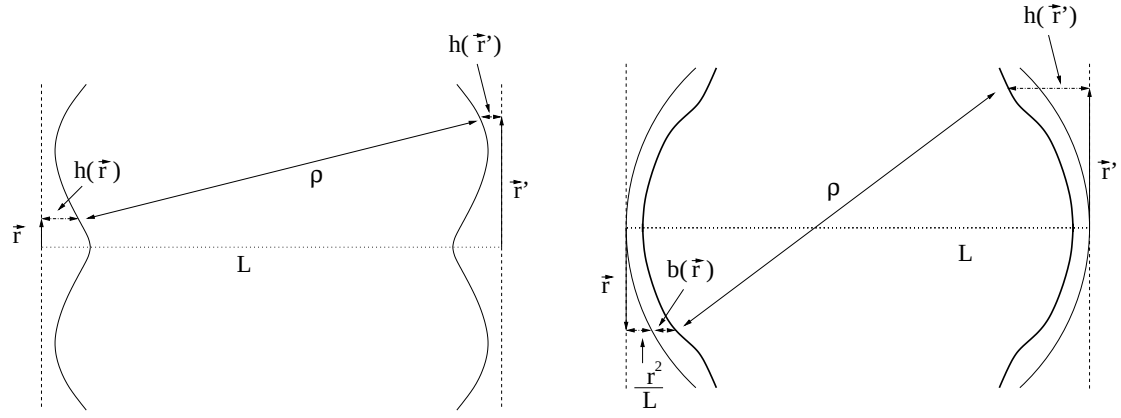

(a) Nearly flat mirrors (b) Nearly concentric mirrors

Figure 2: Geometric constructions for the propagators (3) and (5).

For nearly flat surfaces with profile $h(\vec{r})$ like in Fig. 2(a), using the paraxial approximation we have

$$\mathcal{K}^h_{\mathrm{f}}(\vec{r},\vec{r}\,') = \frac{ik}{2\pi L}e^{-ikL}e^{ikh(\vec{r})}e^{-\frac{ik}{2L}|\vec{r}-\vec{r}\,'|^2}e^{ikh(\vec{r}\,')} \tag{3}$$

Since the mirror heights are measured with respect to flat surfaces, we shall call this the *nearly-flat propagator,* marked by a subscript f. We now consider two deformed concentric mirrors in Fig. 2(b) so that the mirrors height with respect to the flat reference surface is

$$h(\vec{r}) = r^2/L + b(\vec{r})\,; \tag{4}$$

note that concentric spherical mirrors have their radii of curvature equal to $L/2$, and thus a surface height r^2/L. Inserting Eq. (4) into Eq. (2), we obtain another propagator,

$$\mathcal{K}^b_{\rm c}(\vec{r},\vec{r}\,') = \frac{ik}{2\pi L} e^{-ikL} e^{ikb(\vec{r})} e^{+\frac{ik}{2L}|\vec{r}+\vec{r}\,'|^2} e^{ikb(\vec{r}\,')} \tag{5}$$

where $b(\vec{r})$ is the deviation from the concentric spherical mirror; this is called the *nearly-concentric propagator,* marked by a subscript c.
Although we use the terms *nearly-flat* and *nearly-concentric*, it is really not necessary for h and b to be small; in fact, they can give substantial corrections to the mirror shapes with respect to flat and concentric spherical mirrors as long as the resulting mirror surface still satisfies the constraints given by the paraxial approximation.

We consider configurations that are invariant under 180° rotation along the cavity axis. Thus

$$h(\vec{r}) = h(-\vec{r})\,, \qquad b(\vec{r}) = b(-\vec{r})\,.$$

The kernels $\mathcal{K}_{\rm f,\,c}$ are invariant under the transformation

$$\{\vec{r},\vec{r}\,'\} \leftrightarrow \{-\vec{r},-\vec{r}\,'\} \tag{6}$$

or in other words, we have

$$\mathcal{P}\mathcal{K} = \mathcal{K}\mathcal{P}\,, \tag{7}$$

where $\mathcal{P}$ is the parity operator:

$$[\mathcal{P}v]\,(\vec{r}) = v(-\vec{r})\,. \tag{8}$$

Equation (7) implies that all eigenstates can be put into forms with definite parity.

The equivalence relation between a nearly concentric cavity and a nearly flat one is identified by

$$\left[\mathcal{K}^h_{\rm f}(-\vec{r},\vec{r}\,')\right]^* = -e^{2ikL}\mathcal{K}^{-h}_{\rm c}(\vec{r},\vec{r}\,')\,, \tag{9}$$

or

$$\mathcal{P}\left[\mathcal{K}^h_{\rm f}\right]^* = -e^{2ikL}\mathcal{K}^{-h}_{\rm c}\,. \tag{10}$$

Now suppose we have an eigenstate $v_{\rm f}$ of $\mathcal{K}^h_{\rm f}$, i.e., an eigenstate of a cavity with $(+h)$ correction from *flat*, with eigenvalue γ and parity $(-1)^p$:

$$\mathcal{K}^h_{\rm f} v_{\rm f} = \gamma_{\rm f}\, v_{\rm f}\,, \tag{11}$$

$$\mathcal{P} v_{\rm f} = (-1)^p v_{\rm f}\,. \tag{12}$$

Inserting Eqs. (11) and (12) into Eq. (9), we have

$$\mathcal{K}^{-h}_{\rm c} v^*_{\rm f} = e^{-2ikL}(-1)^{p+1}\gamma^*_{\rm f} v^*_{\rm f}\,. \tag{13}$$

	Nearly Flat	Nearly Concentric
Kernel	$\mathcal{K}_{\rm f}^{h}$	$\mathcal{K}_{\rm c}^{-h}$
Eigenstate	$v_{\rm f}$	$v_{\rm f}^{*}$
Parity	$(-1)^{p}$	$(-1)^{p}$
Half-trip eigenvalue	$\gamma_{\rm f}$	$e^{-2ikL}(-1)^{p+1}\gamma_{\rm f}^{*}$
Round-trip eigenvalue	$\eta_{\rm f}$	$e^{-4ikL}\eta_{\rm f}^{*}$

Table 1: Correspondences of propagation kernels, eigenstates, parities, and eigenvalues between dual configurations.

This means, $v_{\rm c} \equiv v_{\rm f}^{*}$ is an eigenstate of $\mathcal{K}_{\rm c}^{-h}$, and thus an eigenstate of a cavity with $(-h)$ correction from *concentric* — the *dual configuration*; the eigenvalue is $\gamma_{\rm c} \equiv e^{-2ikL}(-1)^{p+1}\gamma_{\rm f}^{*}$, and the parity is still $(-1)^{p}$. In this way we have established a one-to-one correspondence between the eigenstates of mutually conjugate configurations (See Table 1).

It is also important to note that the corresponding eigenstates, $v_{\rm f}$ and $v_{\rm f}^{*}$, have the same intensity profiles (on the mirror surfaces) and therefore the same thermal noise averaging properties.

Now for the full propagator, from Eqs. (9) and (7), we have

$$\left[\left[\mathcal{K}_{\rm f}^{h}\right]^{2}\right]^{*} = e^{4ikL}\left[\mathcal{K}_{\rm c}^{-h}\right]^{2} \tag{14}$$

which, from the reasoning above, means that the same duality correspondence exists between eigenstates of the full propagator, and that their eigenvalues are related by

$$\eta_{\rm c} = e^{-4ikL}\eta_{\rm f}^{*} \tag{15}$$

These results can be generalized to the case where the two mirror shapes are not equal , but simply symmetric under 180° rotation. When the field distributions over the mirror surfaces are not equal, we have to define an eigenvalue problem using the round-trip propagator instead of the propagator from one surface to the other. However we can still use the propagators Eq. (3) and Eq. (5) to build a system of integral equations which relate the field distributions $v_1(\vec{r}_1)$ and $v_2(\vec{r}_2)$ over the two mirrors (where the subscript one or two labels the two mirrors) and combine them in round-trip equations. Omitting the cumbersome but straightforward calculations that can be found in [7] I will quote here just the resulting duality relation between the eigenmodes and eigenvectors of the two cavities:

$$\begin{aligned} v_{1c} &= v_{1f}^{*} \quad ; \quad v_{2c} = v_{2f}^{*} \\ \eta_{c} &= e^{-4ikL}\eta_{f}^{*} \end{aligned}$$

This is the generalization of the results found above for the symmetric case; for each mirror we have a duality relation between the nearly-flat and the nearly-concentric configuration if the mirrors profiles calculated with respect to flat reference surfaces

orthogonal to the cavity axis and passing through the centers of the mirrors fulfill this relation:

$$h_{Ac}(\vec{r}) = \frac{r^2}{L} - h_{Af}(\vec{r}) \quad A = 1, 2$$

3 Mexican Hat cavities supporting mesa beams

In this section I give a short introduction to mesa-beams [1],[2],[3] and focus on the work I have done solving numerically the eigenvalue problem for Mexican-Hat cavities in the case of cylindrically symmetric mirrors. The mesa-beam must have an intensity distribution that is nearly flat across the light beam, and then falls as rapidly as possible (to minimize diffraction losses) at the beam's edges. The fastest possible falloff on the mirror surface, for light in an optical cavity of length L, is given by the minimal-Gaussian beam whose radius increases by a factor $\sqrt{2}$ in going from the beam waist (at the cavity's center plane) to the cavity's end mirrors. We therefore superimpose minimal-Gaussian fields whose axes are parallel to the cavity axis and lie within a cylinder of radius D centered on the cavity axis. The non-normalized field distribution over the mirror surface is

$$U(r) = \int_{r' \leq D} \mathrm{d}^2\vec{r}' e^{-\frac{(\vec{r}-\vec{r}')^2(1-i)}{2w_0^2}} = 2\pi \int_0^D e^{\frac{-(r^2+r'^2)(1-i)}{2w_0^2}} I_0\Big[\frac{rr'(1-i)}{w_0^2}\Big] r' \, \mathrm{d}r' \qquad (16)$$

where I_0 is the modified Bessel function of zero order and $w_0 = \sqrt{\frac{L}{k}}$ is the waist of the minimal-Gaussian. To construct the mirror shape which will reflect this mesa beam back to itself (propagating in the opposite direction) we must impose that the surfaces of the mirror coincide with the mesa field's surfaces of constant phase (this is true for infinite mirrors, but also a quite good approximation for finite mirrors if the diffraction losses are small). The resulting height distribution as a function of radius r is given by

$$h_{MH}(r) = \frac{Arg[U(r)] - Arg[U(0)]}{k}$$

The resulting mirror's radial profile is shown in fig. 3(b) along with the spherical (nearly-flat) mirror profile which support a Gaussian beam with the same diffraction losses; notice the shallow bump in the middle and the flaring outer edges which resemble a Mexican hat (sombrero) and give the mirror its name.

Once we have the mirror profile for the optical cavity which can support a mesa beam as its fundamental mode, we can solve the eigenmodes equation (1) and (3) to find the higher modes of this cavity. This is useful in the characterization of this cavity since most of the properties like sensitivity to tilt of the mirrors and stability of the cavity depend on the eigenvalues and field distribution of the modes of the cavity. We will use these results in the next section in the estimation of the impact of the optical torque on the alignment of a Fabry-Perot resonator with non-spherical mirrors. As long as cavity mirrors have cylindrical shapes, we use $h(\vec{r}) = h(|\vec{r}|)$ in

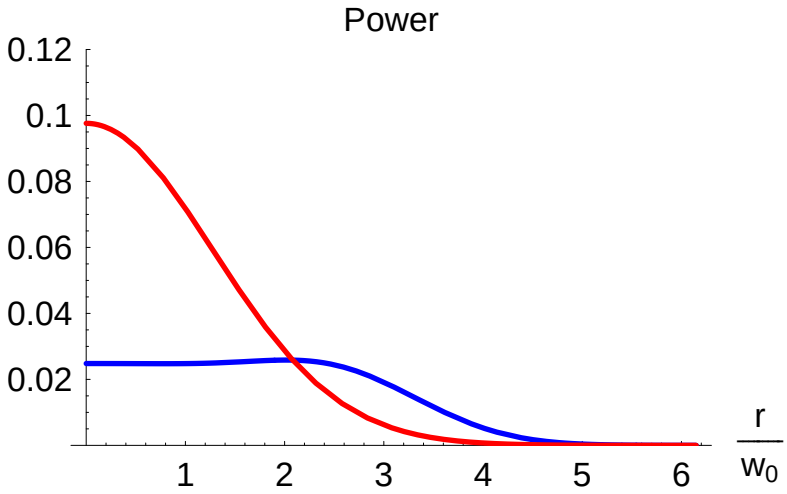

(a) Intensity distributions (a.u.) for a Gaussian beam (**red**) and a Flat Top beam (**blue**) having the same diff. losses.

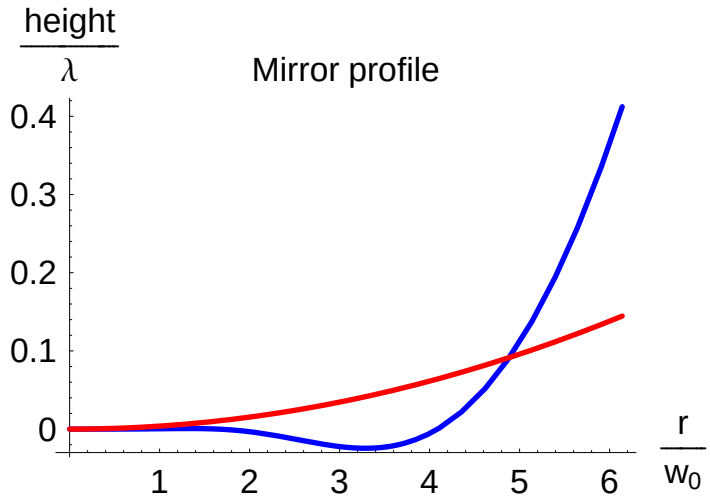

(b) Mirror profiles: spherical mirror (**red**) supporting the Gaussian beam and Mexican Hat mirror (**blue**)supporting the mesa beam.

Figure 3: Comparison between a Gaussian beam and a mesa beam.

the kernel expression Eq. (3). This allows an easy separation of radial and azimuthal degrees of freedom, and simplifies the search for eigenmodes. We adopt the cylindrical coordinate system: $\vec{r} = r(\cos\varphi, \sin\varphi)$. Since $\mathcal{K}$ is now invariant under rotation along the cavity axis, all eigenmodes can be written in the form of

$$v(r,\varphi) = R(r)e^{-im\varphi}\,, \quad m = \text{integer}\,.$$

Inserting this into the eigenequation Eq. (1), and performing analitically the angular integration, we have the radial eigenequation

$$\gamma_{nm} R_{nm}(r) = \int_0^a K^h_{\mathrm{f}(m)}(r,r') R_{nm}(r') r' dr'\,, \tag{17}$$

where for each angular number m we have indexed the eigenstates by n.

$$K^h_{\mathrm{f}(m)}(r,r') = \frac{i^{m+1}k}{L} J_n\left(\frac{krr'}{L}\right) e^{ik\left[-L+h(r)+h(r')-\frac{r^2+r'^2}{2L}\right]} \tag{18}$$

is a symmetric radial kernel, in the *nearly-flat* description [1]. Since $K^h_{\mathrm{f}(m)}(r,r')$ is symmetric, we obtain orthogonality relations between radial eigenfunctions:

$$\int_0^a R_{n_1 m}(r) R_{n_2 m}(r) r dr = \delta_{n_1 n_2}\,.$$

We have thus reduced the problem to a series of one-dimensional integral equation, one for each m. These are homogeneous Fredholm equations of the second kind and there are well documented standard techniques for their numerical solutions. Prominent among these is the Nystrom method, which requires the choice of some approximate quadrature rules in order to reduce the integral equation to a matrix eigenvalue problem of dimension equal to the number of integration points N. It is certainly possible to use low-order quadrature rules like trapezoidal, mid-point or Simpson's rules, but since we are looking for a quite accurate solution of the eigenvalue problem (the modulus of the eigenvalues must be calculated with a precision of at least 10^{-7} for a realistic estimation of the diffraction losses) this would require a large number of integration points and therefore a lot of computation time. I used instead, the Gaussian quadrature rule in order to have a greater accuracy with fewer points. If w_j are the weights of the quadrature rule and the N points x_i are the grid's points on the mirror radius, the equation (17) for a certain m can be written as

$$\gamma R(x_i) = \sum_{j=1}^{N} K(x_i, x_j) x_j w_j R(x_j)$$

Defining R_i the vector $R(x_i)$ and $\widetilde{K}_{ij}$ the matrix $K(x_i, x_j)x_j w_j$ we have transformed the integral eigenvalue problem Eq. (17) to a matrix eigenvalue problem

[1] Here we have used $J_n(z) = \dfrac{1}{2\pi i^n}\displaystyle\int_0^{2\pi} e^{iz\cos\varphi} e^{in\varphi} d\varphi$, in which $J_n(z)$ is the nth order Bessel function of the first kind.

$\gamma\mathbf{R} = \widetilde{\mathbf{K}}\mathbf{R}$ which can be solved for γ and $\mathbf{R}$ by any standard mathematical package (I used Mathematica 5.0). Fig. 4 and Table 2 display some results of this numerical analysis which are used in the stability study that I present in the next section. The frequency distribution of the cavity modes can be calculated using the formula $\Delta\nu_{pq} = \frac{arg(\gamma_p)-arg(\gamma_q)}{\pi}\nu_{FSR}$, where p and q are the mode indexes and $\nu_{FSR} = \frac{c}{2L}$ is the cavity free spectral range. The eigenmodes are not distributed regularly within each free spectral range and from the comparison with the distribution of the eigenmodes for the Gaussian-beam cavity, we expect the mesa beam cavity to be slightly more sensitive to perturbation than the Gaussian-beam counterpart.

γ_{nm}	**m=0**	**m=1**
n=0	0.759686-0.650276i	0.835873-0.548830i
n=1	0.979892-0.199425i	0.984207+0.175787i

Table 2: First eigenvalues for a nearly flat Mexican Hat cavity with $L = 4Km$, $a = 16cm$, $\lambda = 1.064\mu m$ and $D = 4w_0$.

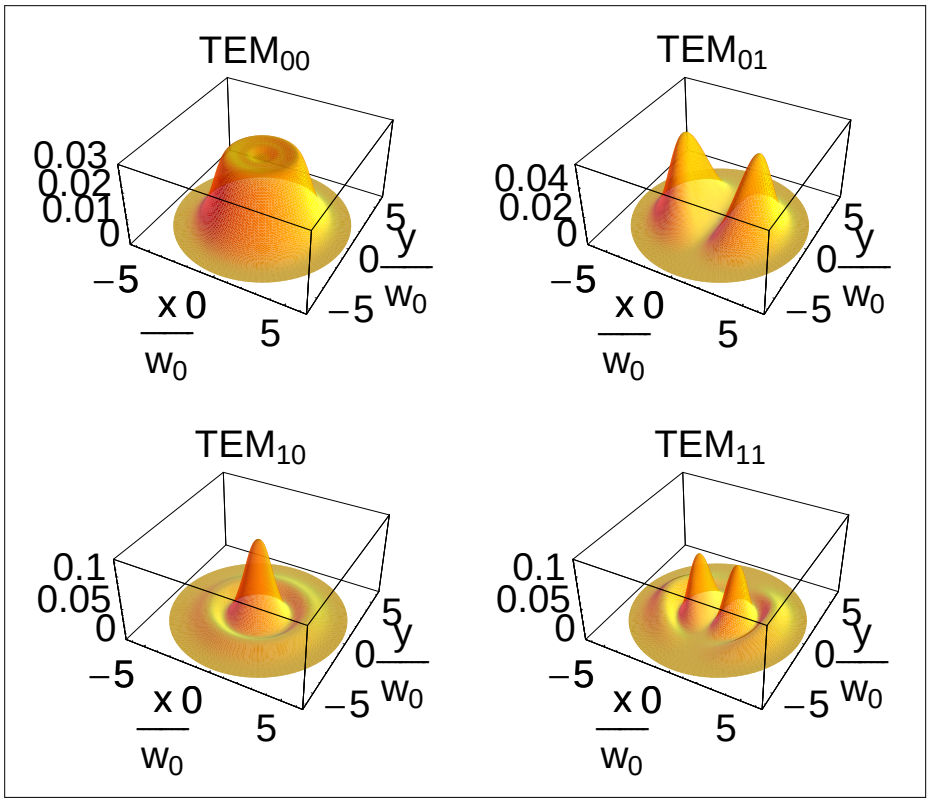

Figure 4: First Mexican Hat cavity modes (power distributions in a.u.): they replace the Gauss-Laguerre modes of the spherical cavities.

4 Radiation Pressure driven instability in MH cavities

This thesis, when completed, will also address dynamical stability issues of Mexican Hat Fabry-Perot cavities, which will include beam profile evolution for changing alignment conditions, evolving radiation pressure effects and other control issues.
It has been recently pointed out [15],[16] that the force induced by radiation pressure, when the end mirrors of an optical resonator are misaligned, can induce a positive feedback and further increase the tilt. This effect is obviously power dependent and increases with power. In the case of anti-symmetric tilt, the coupling between the laser radiation pressure and the misalignment makes the mirrors tilt further, while in the symmetric case the torque induced by the light beam impinging on the mirrors, counteracts the tilt. Although control systems are designed to keep the mirrors aligned, they have limited authority, and minimized coupling between radiation pressure and cavity misalignment is desirable, when there is positive feedback. Quantitative assessments of the problem (that depends on the geometry of the resonator) have shown that optical cavities with almost flat mirrors are more prone to this instability with respect to almost concentric cavities (where the comparison is done between geometrical configurations that correspond to the same transverse distribution of the fundamental mode on the reflective surface of the mirrors). In Fig.5 there is a geometrical explanation of this phenomenon for the spherical mirror case.

Because of this issue, the current baseline design for Advanced LIGO has been changed from nearly flat to nearly concentric. It is important to evaluate the radiation pressure problem also for mesa beams. We do so using the results of the two previous sections. We will use our proved duality-relation to show that, in the quasi-concentric Mexican-Hat configuration, the cavity is less prone to become unstable and therefore easier to control [8]. For general, non-spherical cavities, a perturbative approach must be used to calculate the tilt instability. The torque due to radiation pressure is expressed in terms of numerically found eigenvalues and intensity profiles of the cavities's spatial eigenmodes. In particular, we write the fundamental mode of the tilted cavity as a superposition of the lowest order modes of the unperturbed cavity $v_{tilt} = v_{00} + \alpha v_{01}$ (in the first order approximation) where the coupling parameter α is a function of the unperturbed quantities $\gamma_{00}, \gamma_{01}, v_{00}, v_{01}$. Then the radiation pressure torque itself can be written as a function of the unperturbed quantities introduced above. Without going into the details of the calculations I quote just the final results. Using the numerical work done for the mesa beam in the nearly flat configuration, and using the mapping of eigenvalues and eigenmodes between the nearly flat and nearly concentric cavities (to obtain the estimation of the tilt instability for nearly concentric Mexican-Hat cavities without having to solve the eigenvalue problem again) we proved that the nearly concentric MH configuration is much more stable than the nearly flat MH one, and even slightly more stable than the corresponding nearly concentric spherical configuration proposed for Advanced LIGO.

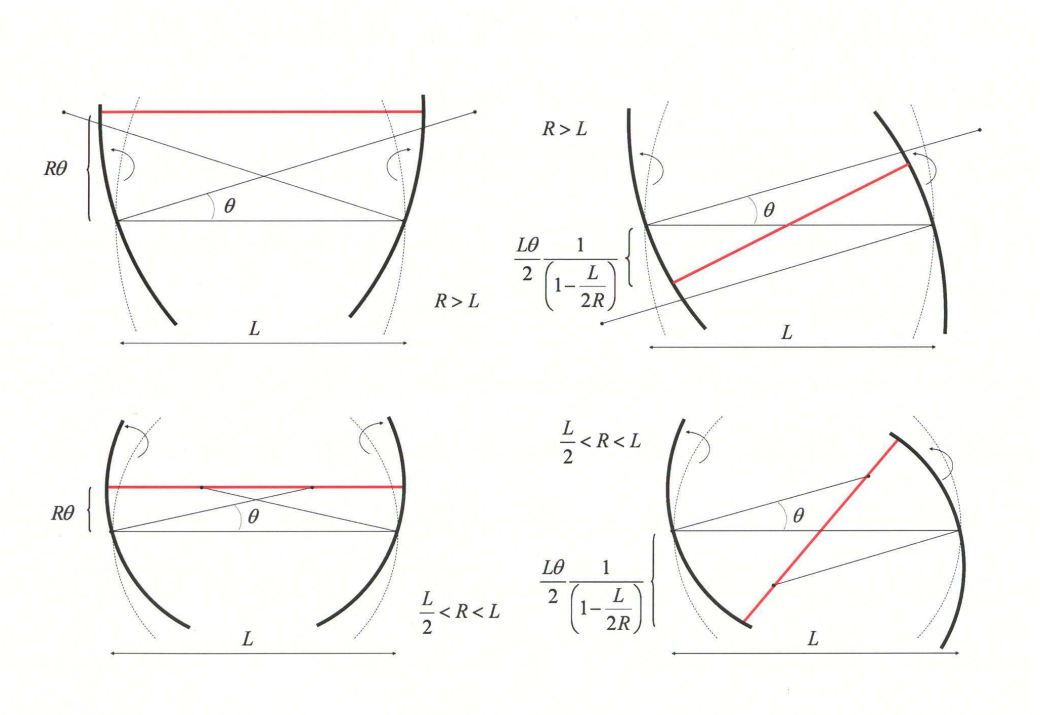

Figure 5: Each of these optical resonators is formed by two identical spherical mirrors, with radius of curvature much larger (nearly flat cavity) and smaller (nearly concentric) then the distance between the optics. When the mirrors are tilted in a common mode (on the left) by an angle θ the optical axis shifts by $R\theta$. The resulting torque is smaller in nearly concentric cavities than in nearly flat resonators. The torque restores the cavity alignment when the mirrors are tilted in a differential mode (on the right). The change in the optical axis is a rotation $\theta/(1-\frac{L}{2R})$ around the center of the cavity. The resonating beam is displaced by $\frac{L\theta}{2}/(1-\frac{L}{2R})$ on the optics. This displacement occurs in opposite directions and tends to restore the correct alignment. Since this rotation is larger in nearly concentric cavities, these benefit more from the restoring torque. Quantitative assessments can be found in literature and substantiate these considerations [15, 16]

5 Thermal noise: finite mirrors

In this section I present my ongoing work [14] on a precise comparative estimation of the various thermal noise contributions (Brownian and thermoelastic for both coating and substrate) for finite sized mirrors. It is essential to evaluate accurately the balance of these effects to optimize the sizes of the substrates, and make suitable choices of material for the advanced detectors. Moreover we make a detailed analysis of the suppression of the thermal noises we can achieve using the Flat Top beam instead of the Gaussian beam. In literature there are partial studies on thermal noise for finite mirrors and almost nothing about the actual improvements we can obtain by switching to Mexican Hat cavities.
My analysis is based on the Levin's direct approach to calculate the mirror's thermal noise. My calculations are based on the analytical solution for the elastic problem of a cylindrical mirror with the appropriate boundary conditions, found by Liu and Thorne in their study of thermoelastic and Brownian thermal noise in finite sized mirrors [10]. I used their solution for the displacement field for the test masses substrate in order to extend the analysis of the coating thermal noise done by G.Harry et al. [12] to the case of finite sized mirrors.
The importance of an analytical formula, which enters in the noise calculation through the strain tensor, the stress tensor and the expansion (for coating and substrate), is that we can more easily study the realistic behavior of all the thermal noises as we change the mirror aspect ratio, its mass, and/or the beam radius.
I conducted a comparative study of the thermal noise in different mirror configurations, both for Fused Silica and Sapphire, which are the two candidates for the substrate of the Advanced LIGO test masses. I kept fixed the mirror mass to 40 Kg, the requirement for Advanced LIGO to reduce the impact of radiation pressure noise. I built a Mathematica notebook in which all the functions that enter in the thermal noise calculation are written as functions of the mirror radius: the mirror thickness is dynamically adjusted as a function of the mirror radius to maintain the total mass fixed and the Gaussian beam radius is also dynamically calculated as function of the mirror radius to maintain a fixed diffraction loss (I chose 10^{-6} and used the clipping approximation for the calculation of diffraction losses). I made the calculation for the noise spectral densities at the frequency of 100 Hz, and, assuming the quasi-static approximation for the oscillations of stress and strain in the test masses and material properties independent from frequency (not bad approximations in the Advanced LIGO detection band), we have that the strain sensitivity for the substrate thermoelastic noise scales as $1/f$ while the strain sensitivity for substrate and coating Brownian thermal noise scales as $1/\sqrt{f}$. In the calculations we used the present most probable values for the material's physical constants (losses, thermal conductivity, Young modulus,...)[14]. Since the formulas are long and complicated I skip the details of the calculations and I will present only the results in the following graphics, where h is the strain sensitivity (equivalent noise) calculated for one mirror of a 4 Km long optical cavity. In the first two graphs 6(a),6(b) I kept the different contributions to thermal noise separated and plotted the corresponding behavior for the infinite

mirror case (dashed lines) as a comparison; the infinite mirror plots are calculated using the beam radius chosen for the finite mirror case to satisfy the $1ppm$ diffraction loss constraint.

As expected, the dominant contribution for Fused Silica test masses comes from the coating thermal noise, whereas for Sapphire substrate the dominant noise source is the thermoelastic effect. To calculate the optimized mirror's aspect ratio and beam radius we added quadratically the three noise sources.
The results for Gaussian beams are shown in Fig.7(a) and Fig.7(b): the two curves present a minimum for different values of the mirror radius and, although the Advanced LIGO baseline mirror aspect ratio choice for Sapphire (15.7 cm mirror radius) is well optimized, the optimized geometry for Fused Silica would require a radius of about 18.3 cm; this would correspond to a gain of about 8% in h and $\sim$ 24% in detection rate.

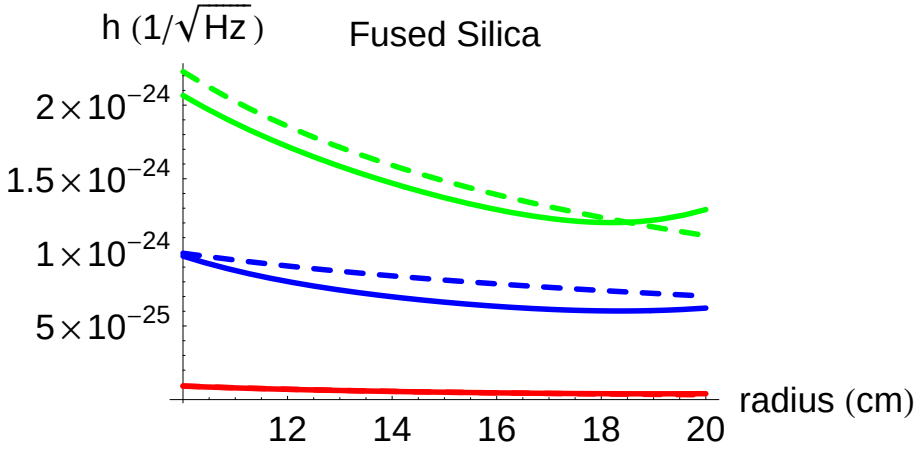

(a) Different thermal noise contributions for Fused Silica substrate and $Ta_2O_5 + SiO_2$ coating

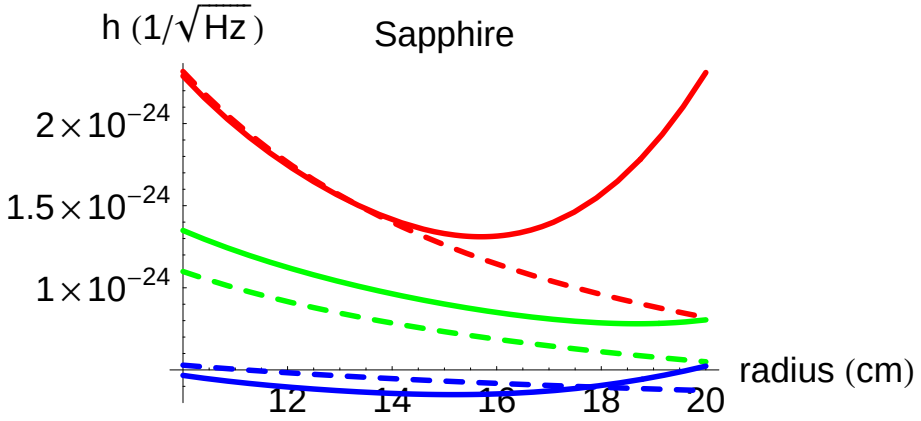

(b) Different thermal noise contributions for Sapphire substrate and $Ta_2O_5 + SiO_2$ coating

Figure 6: Thermal noises for Gaussian beam: substrate thermolelastic (**red**), substrate Brownian (**blue**) and coating Brownian (**green**)

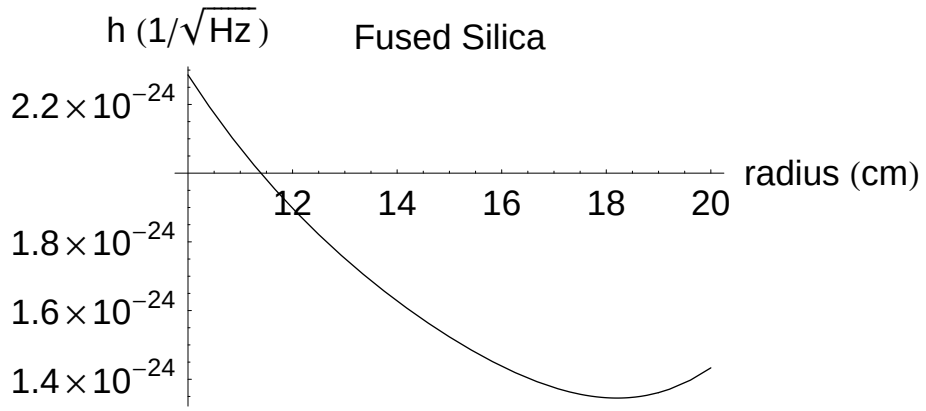

(a) Dependence of "total" thermal noise on the mirror radius

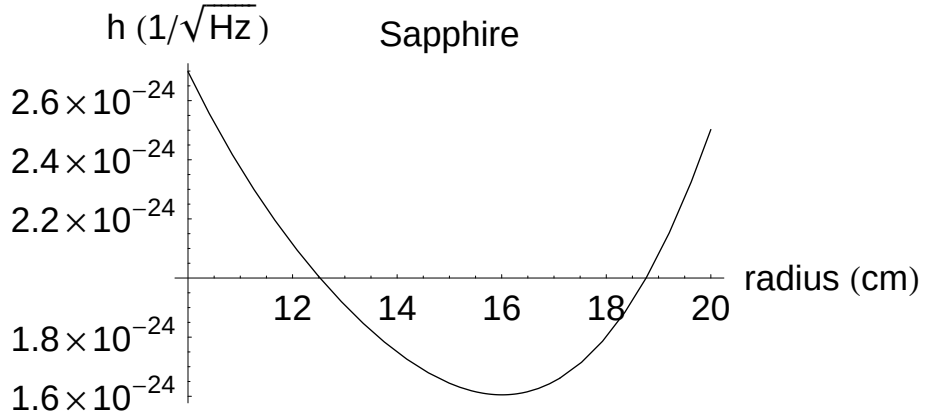

(b) Dependence of "total" thermal noise on the mirror radius

Figure 7: Mirror's aspect ratio optimization for Gaussian beams.

5.1 Thermal noise for mesa beam

In this section I present some preliminary results I have obtained during the last weeks on the calculation of thermal noise in finite sized mirror when using a mesa beam to sample the surface of the test mass. This work is particularly important for further improvements of the Advanced LIGO project because there are no complete calculations of the amount of noise reduction that can be achieved by implementing a mesa beam, for the different types of thermal noises. Since the construction of Advanced LIGO will freeze its mirror's aspect ratio, it is important to understand early on if the mesa beam requires drastically different mirror aspect ratios. I used the same techniques described for the Gaussian beam case, dynamically changing the mirror radius and the mesa beam profile in order to keep the diffraction losses at 1 ppm (this allows a meaningful comparison between the two optical systems) and adjusting the mirror thickness in order to maintain the total mass fixed. In this case the calculations are somewhat more complicated than in the Gaussian beam case because, as shown in equation Eq. 16, the beam profile has the form an integral equation (not analytically integrable) and this slows down all the processes for the calculation of thermal noises. I decided to make the calculations only for a discrete set of mirror radius ranging from $12cm$ to $21cm$ (step $1cm$). The results are shown in the graphs 8(a) and 8(b).

The total thermal noise for Gaussian beam and Flat Top beam are shown in Fig. 9. The comparison between the two, points out a considerable improvement in sensitivity for the gravitational wave detector if the mesa beam is used in place of the standard Gaussian beam; since the improved sensitivity is of about a factor 1.6 for Sapphire and 1.7 for Fused Silica (at the minima), the Flat Top beam configuration is in any case a very interesting option for the future interferometers. It should also be noted that a wider thinner mirror optimizes the performances of Mexican Hat mirrors.

This work is still in progress and still receiving many inputs from the Advanced LIGO community which is very interested in this type of analysis. Future developments include the addition of the thermoelastic coating noise, sensitivity optimization allowing larger diffraction losses (i.e. 5-10 ppm and estimate the impact of this in the thermal noise calculations for Gaussian and Flat Top beam), extend the analysis to the case in which the loss angle and the elastic properties of the coating are not isotropic. It is important to stress, however, that the choice of appropriate material parameters for the multi-layer coatings is a difficult subject since the thermo-physical properties of their materials in a film form are not well characterized and this introduces limitations to the quantitative statements about the resulting thermal noises.

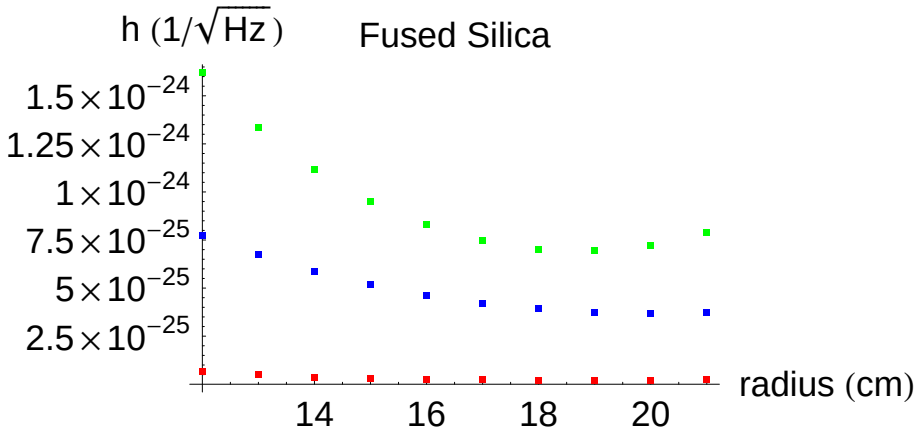

(a) Different thermal noises for Fused Silica substrate and $Ta_2O_5 + SiO_2$ coating

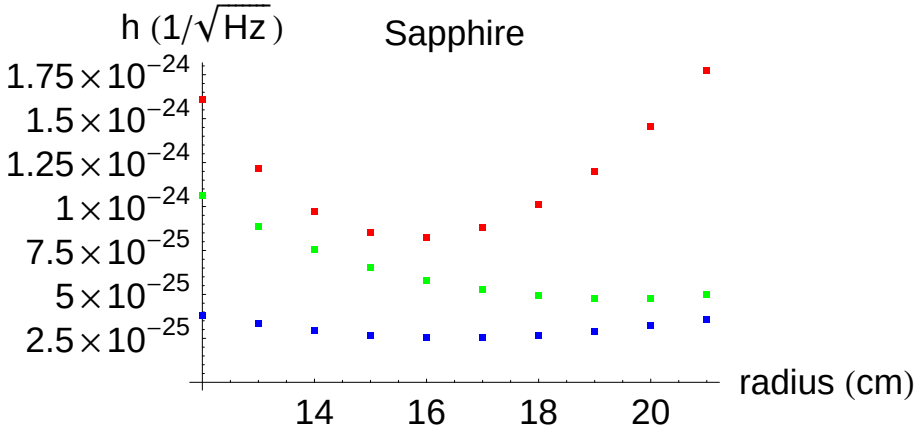

(b) Different thermal noises for Sapphire substrate and $Ta_2O_5 + SiO_2$ coating

Figure 8: Thermal noises for mesa beam: substrate thermolelastic (**red**), substrate Brownian (**blue**) and coating Brownian (**green**)

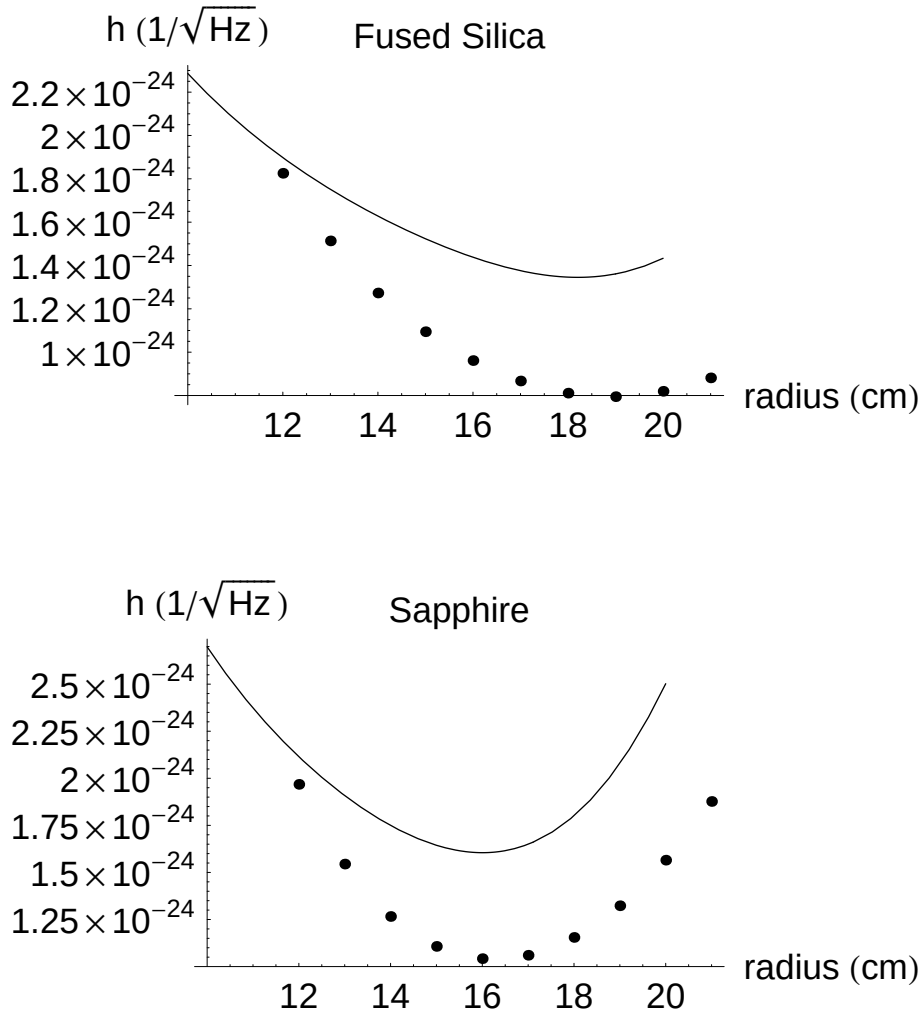

Figure 9: Gaussian beam (**solid line**) vs. Mesa beam (**dots**) "total" thermal noise.

6 Flat-Top beam cavity prototype test

This work is a collaboration with E. D'Ambrosio, R. DeSalvo, J.M. Mackowski, M. Mantovani, A. Remillieux, B. Simoni, M. Tarallo and P. Willems, colleagues at University of Pisa, the LIGO Laboratory at Caltech and LMA in Lyon. The main motivation of this project is to demonstrate the feasibility of building a Fabry-Perot cavity which can support a Flat-Top beam [17]. This cavity prototype has been designed to study how efficiently a Mexican Hat cavity can transform an incoming Gaussian beam into a Flat-Top beam profile and represents a scaled down version of the Advanced LIGO cavities. The prototype is a 7.3m long, rigid, folded cavity, with finesse 100, suspended under vacuum. The mechanics is built using INVAR, a material with low thermal expansion coefficient. Since ground vibrations can excite resonances in our interferometer structure and disturb the operation, the cavity is suspended by a system of four maraging wires for horizontal isolation and GAS (Geometric-Anti-Spring) blades for vertical isolation. For optical stability and thermal isolation the entire system is enclosed in a vacuum tank. The production of the Mexican Hat mirror is under the responsibility of our colleagues at LMA-Lyon. The mechanical part of this experiment works properly; tests made with spherical optics show that our device is working as designed. Mexican Hat mirrors are expected to be delivered in the next future.

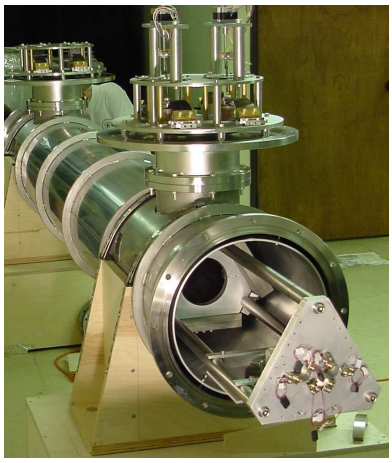

(a) Picture of the apparatus.

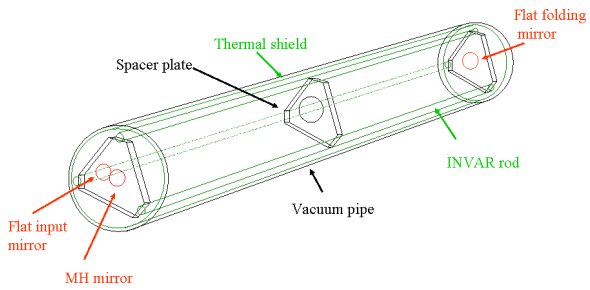

(b) Schematic diagram of the cavity prototype

Figure 10: Flat Top beam cavity prototype.

My main contributions to this project are [18](as well as sporadic lab assistance) the theoretical predictions, using the same techniques I explained in Sec. 3, of the cavity modes we will observe in the Mexican Hat configuration (as soon as the Mexican Hat mirror will be available) and the theoretical analysis about the sensitivity of the cavity to misalignments effects. I did these evaluations using two different approaches: the first is a perturbation theory based on the definition of an unperturbed and a perturbed eigenvalue problem, and the second is a dynamical simulation of what really happens in an optical cavity when an initially launched field is reflected

back and forth between the misaligned mirrors until a steady-state field distribution is obtained (this technique was already used in the past to study the resonant modes in aligned and misaligned spherical resonator). As soon as data will be available we will proceed to a detail comparison between data and my predictions.
Making actual tests of radiation pressure effects (Cf. Sec. 4) on suspended masses would require to build a very expensive high power interferometer, with a price comparable with a LIGO interferometer. Simulations will be of limited reliability, due to the complexity of the problem.
We will attempt to use the prototype to perform an hybrid simulation in which the larger mesa beam will be replaced by our small one. We will then use the beam profile monitors to calculate in real time the radiation pressure corresponding to large, high power, beams, and its effect on large, suspended and controlled test masses. Then we would calculate a scaled actuation response to apply to the piezos controlling our mirrors. This configuration will allow the fixed mirrors in our rigid cavity, to "fly" as if they were real suspended masses under high power conditions. Monitoring the beam evolution under different (simulated) power and control conditions may produce a credible simulation of real interferometers. This ambitious program, based on my simulations, may either fall inside or outside the time constraints of my graduate studies.

References

[1] E. D'Ambrosio, R. O'Shaughnessy, S. Strigin, Kip S. Thorne, S. Vyatchanin and P. Willems "*Advanced LIGO: non gaussian beams*" Classical and Quantum Gravity (2004) Vol.21 N.5 867

[2] E. D'Ambrosio "*Non-spherical mirrors to reduce thermoelastic noise in advanced gravity wave interferometers*" Phys.Rev.D Vol.67 (2003) ID 102004

[3] E. d'Ambrosio, R. O'Shaughnessy, S. Strigin, K.Thorne, and S. Vyatchanin, "Reducing Thermoelastic Noise in Gravitational-Wave Interferometers by Flattening the Light Beams", Phys. Rev. D, submitted.

[4] D. Shoemaker, "Advanced LIGO: Context and Overview (Proposal to the NSF)", LIGO-M030023-00, 2003; available at http://docuserv.ligo.caltech.edu/

[5] A.G.Fox and T.Li *The Bell System Technical Journal* Vol.40, pp.453-488 (1961)

[6] A.E.Siegman *Lasers* University Science Books (1986)

[7] J. Agresti, E. D'Ambrosio, Y. Chen, and P. Savov, Phys. Rev. D, in preparation

[8] J. Agresti and E. D'Ambrosio, "Equivalence relation between non spherical optical cavities and application to advanced G.W. interferometers",to be published in the GR17 proceedings and available at http://docuserv.ligo.caltech.edu/ as LIGO-G040307-00-R.

[9] V. Braginsky, M. Gorodetsky, and S. Vyatchanin, Phys. Lett. A **264**, 1 (1999).

[10] Y. T. Liu and K. Thorne, Phys. Rev. D **62**, 122002 (2000).

[11] Y. Levin, Phys. Rev. D, **57** N.2 659 (1998).

[12] G. M. Harry *et al.*, Class. Quantum Grav. **19** 897 (2002).

[13] V. Braginsky and S. Vyatchanin , Phys. Lett. A **312**, 244 (2003).

[14] J. Agresti and R. DeSalvo, " Study of mirror thermal noise as a function of mirror aspect ratio and size", draft available at http://docuserv.ligo.caltech.edu/ as LIGO-T040203-00-R.

[15] D. Sigg, "Angular Instability in High Power FP Cavities", LIGO-T030120-00, 2003; available at http://docuserv.ligo.caltech.edu/

[16] J. Sidles and D. Sigg, "Optical Torques in Suspended Fabry-Perot Interferometers", LIGO-P030055-B, 2003; available at http://docuserv.ligo.caltech.edu/

[17] B. Simoni, Tesi di Laurea Specialistica, available at http://docuserv.ligo.caltech.edu/as LIGO-P040037-00-R.

[18] J. Agresti *et al.*, "Flat-Top Beam Profile Cavity Prototype", to be published in the GR17 proceedings and available at http://docuserv.ligo.caltech.edu/as LIGO-G040306-00-R.